Eur. Phys. J. D **4**, 335–342 (1998)

**THE EUROPEAN PHYSICAL JOURNAL D**



# Photoionization of argon, krypton and xenon clusters in the inner valence shell region

R. Thissen[1,a], P. Lablanquie[1], R.I. Hall[2], M. Ukai[3], and K. Ito[4]

[1] LURE, Université Paris-Sud, 91405 Orsay, France
[2] DIAM, Université Pierre et Marie Curie, 4 place Jussieu, BP 75, 75252 Paris, France
[3] Department of Applied Physics, Tokyo University of Agriculture and Technology, Nakacho 2-24-16, Koganei-shi, Tokyo 184, Japan
[4] Photon Factory, Institute of Materials Structure Science, High Energy Accelerator Research Organization (KEK), 1-1 Oho, Tsukuba, Ibaraki 305, Japan

Received: 10 February 1998 / Revised: 17 July 1998 / Accepted: 31 July 1998

**Abstract.** Photoionization of rare gas clusters in the innervalence shell region has been investigated using threshold photoelectron and photoion spectrometers and synchrotron radiation. Two classes of states are found to play an important role: (A) valence states, correlated to dissociation limits involving an ion with a hole in its innervalence *ns* shell, (B) Rydberg states correlated to dissociation limits involving an ion with a hole in its outervalence *np* shell plus an excited neutral atom. In dimers, class A states are "bright", that is, accessible by photoionization, and serve as an entrance step to form the class B "dark" states; this character fades as the size of the cluster increases. In the dimer, the "Mulliken" $E\,^2\Sigma u^+$ valence state is found to present a shallow potential well housing a few vibrational levels; it is predissociated by the class B Rydberg states. During the predissociation a remarkable energy transfer process is observed from the excited ion that loses its innershell electron to its neutral partner.

**PACS.** 36.40.-c Atomic and molecular clusters – 36.40.Wa Charged clusters

## 1 Introduction

The photoionization of clusters is still much less well-known than that of its constituent atoms or molecules. Among the reasons for this situation is the high flux necessary to sample these diluted species and the high energy resolution needed to resolve their vibrational structure, characteristics that are only now becoming routinely accessible in Synchrotron Radiation laboratories. Rare gas clusters illustrate this perfectly: ionization in the outer valence *np* shell (where *np* stands for 3*p* in Ar, 4*p* in Kr, and 5*p* in Xe) is now quite well-known. Cross-sections for the ionization process have been investigated with mass spectrometers [1]. Photoelectron spectroscopy studies [2,3] have increased in resolution up to that attained by the threshold photoelectron technique which has succeeded in observing vibrational progressions of homonuclear rare gas dimer ions [4–6]. Multiphoton laser ionization has recently entered the field with its even higher resolution capabilities [7]. Finally, the stability and dissociation reactions of rare gas cluster ions has also been investigated with threshold photoelectron/ion coincidences techniques [8] or with double focusing mass spectrometers [9]. These many observations have served to motivate calculations of potential surfaces of the electronic states involved [10–13].

Ionization of rare gas clusters in the inner valence *ns* shell is much less well-known. The first theoretical consideration of the problem was given by Mulliken [10], who predicted that ionization of rare gas dimers in the ns shell should give rise to two electronic states, an "almost certainly" stable one, $E\,^2\Sigma_u^+$, corresponding to the removal of a $\sigma_u$ *ns* electron, and a "certainly" repulsive one, $F\,^2\Sigma_g^+$, corresponding to the removal of a $\sigma_g$ *ns* electron. The first experiment that set out to investigate these states was that of White and Grover [14], who, by mass spectrometry techniques, observed the Rydberg series converging to the above states in the $Ar_2$ and $Kr_2$ clusters, as well as to the corresponding states in the trimers. The potential well of the bound $E\,^2\Sigma_u^+$ state was estimated to be 47(3) meV in $Ar_2$ and 104(22) meV in $Kr_2$. Such an investigation was extended to heteronuclear rare gas clusters by Castex *et al.* [15]. Subsequently, Cachoncinlle *et al.* [16] performed *ab initio* calculations of the excited electronic states of $Ar_2^+$; they could "find no evidence of bound states correlated with $Ar^+(3s^13p^6)$ + Ar″ but discovered, on the contrary, in this energy range, many "Rydberg excited electronic states of $Ar_2^+$" correlated with $Ar^+(3p^5,\ ^2P)$ + $Ar^*(3p^54s,\ ^{3,1}P)$. The form of these new states is quite original: at large internuclear distances resonant

[a] e-mail: thissen@lure.u-psud.fr

transfer of the Rydberg "4$s$" electron from one $Ar^+$ centre to the other causes wells of 0.6−0.8 eV around $R = 4-5$ Å (compared with $R_e = 3.76$ Å for the neutral $Ar_2$ dimer ground state [17]). At small internuclear distance, local minima around $R = 2$ Å correspond to configurations with an outer Rydberg electron orbiting around an $Ar_2^{++}$ [18]. Later, threshold electron-ion coincidence experiments done by the group of Kamke [19–22] confirmed the existence of these peculiar states and showed that they can be interpreted as the seed of excitons in bigger rare gas clusters. These states were also observed to play an important role in ion desorption from condensed Ar [23]. For this reason, and in order to bear in mind their special shape, we will call "excitonic states" these excited Rydberg states of the rare gas dimers, discovered by Cachoncinlle *et al.* [16].

Apparently, a contradiction seems to emerge from this overview: the stable $E\ ^2\Sigma_u^+$ state, correlated to the $Ar^+(3s^1 3p^6)$ + Ar limit, predicted by Mulliken [10] was thought to be observed in the experiments of White and Grover [14] but sophisticated *ab initio* calculations found no evidence for such a loosely bound state. Instead, these calculations discovered more tightly bound "excitonic" states. In order to try and resolve this ambiguity, we have re-examined the energy range in question by means of two different instruments both based on synchrotron radiation: (1) a threshold electron spectrometer, used to locate the excited electronic states of the rare gas cluster ions $Rg_n^+$, (2) an electrostatic analyzer that measured the kinetic energy of fragment ions from the dissociation of $Rg_n^+$ cluster ions.

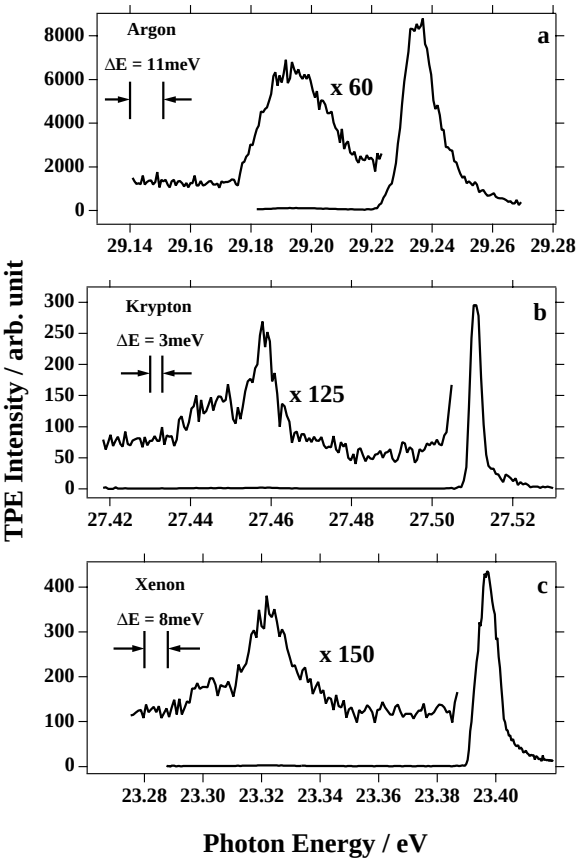


**Fig. 1.** Threshold photoelectron spectra obtained at low stagnation pressure, showing the dimer and monomer contributions. Typical count rates on the maximum of a small peak (dimer contribution) was 1 count/s.

## 2 Experimental method

Rare gas clusters were produced in a supersonic jet obtained by expansion of the gas through a 30 $\mu$m nozzle; stagnation pressures were varied from 0.7 to 6 atm in order to change the size distribution of the clusters. The gas beam was unskimmed and expanded directly into the experimental chamber, in front of a 20 000 $Ls^{-1}$ cryopump. The interaction region was located 10 mm above the nozzle, where the cluster beam intercepted the photons from beam line 20 A of the synchrotron radiation source of the Photon Factory. Beam line 20 A is equipped with a 3 m normal incidence monochromator [24] and with either a 1200 lines/mm or a 2400 lines/mm grating. Depending on the intensity of the signal, the slits of the monochromator were varied from 10 $\mu$m up to 1 mm, implying a wide range of photon resolution. The highest resolution scan was obtained in Kr (see Fig. 1) and used 20 $\mu$m slits and the 2400 lines/mm grating for a resolution of 0.05 Å. As cluster species are only a small part of the gas beam which is by far dominated by isolated atoms, calibration of the photon energy was conveniently obtained from the atomic features in the threshold electron or ion yield spectra.

In order to extract the weak signal associated with the clusters from the dominant one due to the atoms present in the jet, two very sensitive spectrometers were used:

- A threshold electron spectrometer with a resolution better than 4 meV [6] recorded spectra in the photon energy domain where no atomic contribution is present, that is, in the region roughly 5 eV below the $Rg^+(ns^{-1})$ threshold. A detailed description of this spectrometer can be found in references [5,6,25,26]. Briefly, it consists of a stack of electrostatic lenses that generate, by field penetration into the interaction region, a shallow potential trap for low energy electrons. These "threshold" electrons are then guided to and focused at the entrance of a hemispherical analyzer in which they are separated from energetic electrons. Note that no time filtering of the high energy electrons was used here. This technique can improve the optimal resolution of the spectrometer and discriminate more efficiently against energetic electrons [6], but was not found necessary here in view of the limited photon energy resolutions used.
- An electrostatic spectrometer for the measurement of the kinetic energy of fragment ions from the dissociation of $Rg_n^+$ cluster ions. The idea was here to use the fact that ionization of rare gas atoms creates ions with thermal energies only, any energetic ions coming necessarily from dissociation of a cluster ion. This spectrometer has been used previously in the Photon Factory laboratory in various ion kinetic energy

experiments [27,28] and has been described in detail in these references; briefly, it consists of an electrostatic lens system, a dispersive element of parallel plate type and a position sensitive detector. This system allows the complete kinetic energy spectrum to be recorded without changing any potential of the analyzing system. Note that kinetic energies of fragment ions are measured independently of their mass.

## 3 Results

### 3.1 Threshold photoelectron spectra

Figure 1 shows threshold photoelectron spectra obtained at low stagnation pressures for the three rare gases studied. The dominant peak corresponds to ionization of the isolated atom in the ns shell, and provides an easy calibration of the photon energy scale [29]. The asymmetric shape, given by the convolution of the photon energy distribution with the transmission function of the threshold electron spectrometer, is due to the imperfect rejection of more energetic electrons ($< 20$ meV) The "practical" overall resolution, given by the width of the atomic peak, amounts here to 8, 3 and 11 meV for Xe, Kr and Ar, respectively. The difference in resolution comes exclusively from the setting of the monochromator, the settings (slit widths + grating) were, respectively: (100 $\mu$m + 2400 lines/mm), (20 $\mu$m + 2400 lines/mm) and (10 $\mu$m + 1200 lines/mm).

The signal at the low photon energy side of the $ns^{-1}$ peaks in Figure 1, which is two orders of magnitude less intense than the atomic contribution, arises from clusters and is attributed to the dimer component for two main reasons. First, the stagnation pressure (0.8 atm for Xe, 1.5 atm for Kr and 2 atm for Ar) was made as low as possible in order to minimise the relative abundance of large clusters, while preserving a tractable signal. Second, the width of the observed structures, which is comparable to that of the atomic line, suggests they originate from the dimer rather than from a larger cluster which would more likely give rise to broad, structureless bands. Furthermore, the intensity ratio of the dimer to monomer signal is roughly comparable to the one observed under similar conditions with the same set-up in the *np* threshold region [6]. The similarity between features observed in the three rare gases and their location just below the *ns* main line naturally suggests that this dimer structure is related to a process involving the ionization of an ns inner-valence electron in a dimer. Consequently, this structure is attributed to ionization into vibrational levels of the bound $E\ ^2\Sigma_u^+$ state correlated to the $Rg^+(ns^{-1})$ + Rg limit.

The evolution of the threshold photoelectron spectra with stagnation pressures is shown in Figure 2. Note that only the cluster signal is shown here, the peak at high photon energy, most prominent in the low pressure curves, corresponds, in all three cases, to the structure attributed to the $E\ ^2\Sigma_u^+$ state of the dimer in Figure 1. Figure 2 shows the appearance of broad bands when the average

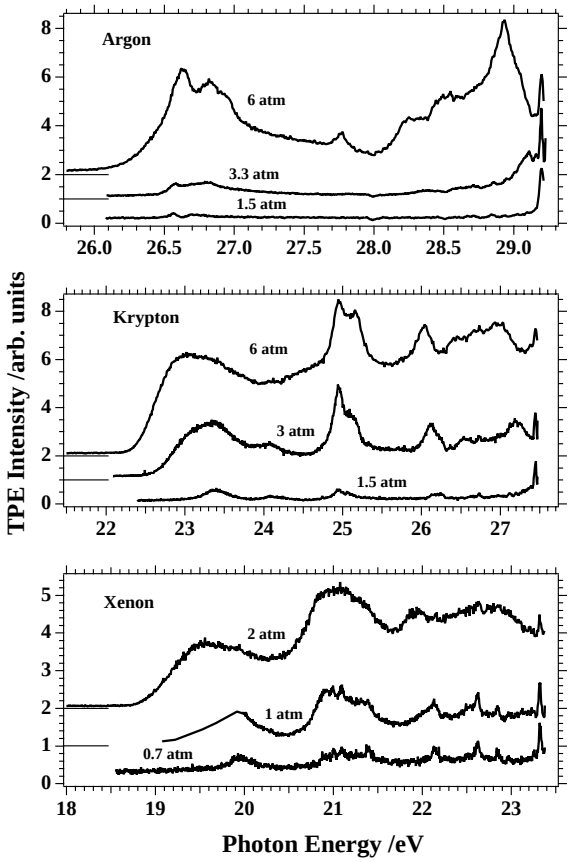


**Fig. 2.** Evolution of the threshold photoelectron spectra with stagnation pressure for Ar (a), Kr (b) and Xe (c). The monochromator slits were throughout 10 $\mu$m with a 1200 lines/mm providing a 1 Å resolution. Accumulation time was 5 hours for each curve.

cluster size $N_{av}$ increases. This average cluster size for the three curves shown for each of the rare gases in Figure 2 vary as 1:5:16 for Ar, 1:4:16 for Kr, and 1:2:8 for Xe, using a rough model [30,31] to estimate these numbers from the experimental conditions. Absolute values cannot be easily derived but are estimated to be between 1 and 2 for the lowest pressure curves in each case, hence the interpretation of a dominant dimer contribution under the lowest pressure conditions.

The threshold electron signal in the range 3−5 eV below the atomic $Rg^+(ns^{-1})$ ionization limit can be attributed to formation, in large clusters, of the excitonic states analogous to those predicted by Cachoncinlle *et al.* for the Ar dimer [16]. The low energy threshold of the signal in Ar is around 26.2−26.4 eV. Comparison of these values with the calculations of Cachoncinlle *et al.* [16] suggests that, in the $Ar_N$ cluster, we observe the formation of the lowest excitonic state in its potential well at large internuclear separation. The good agreement between our measurement and the value of Cachoncinlle *et al.* [16] for the position of this well in the dimer, calculated near 26.5 eV, also implies that the stabilisation of this well with

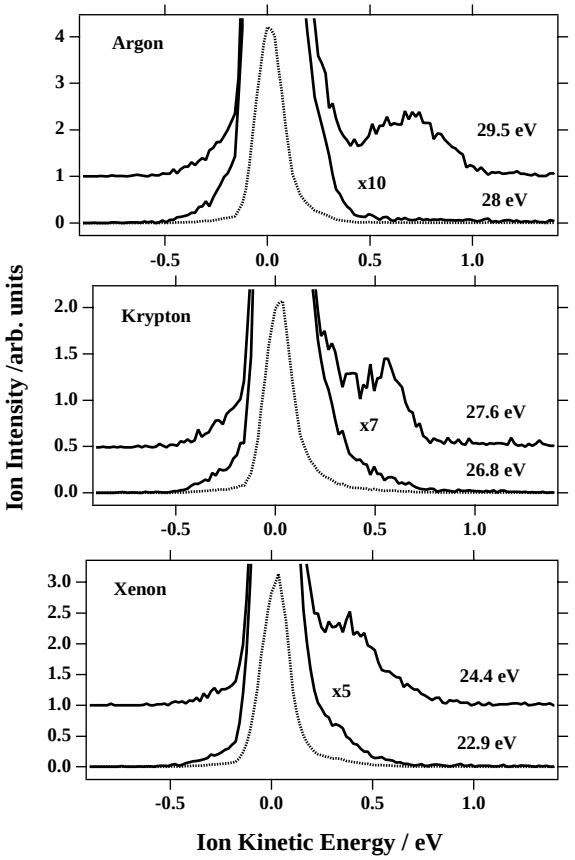


**Fig. 3.** Ion kinetic energy spectra. For each gas, two spectra obtained at different photon energies are presented. A multiplication factor is used to display the energetic ion signal. Count rate on the maximum of the energetic component was a few counts/10 s.

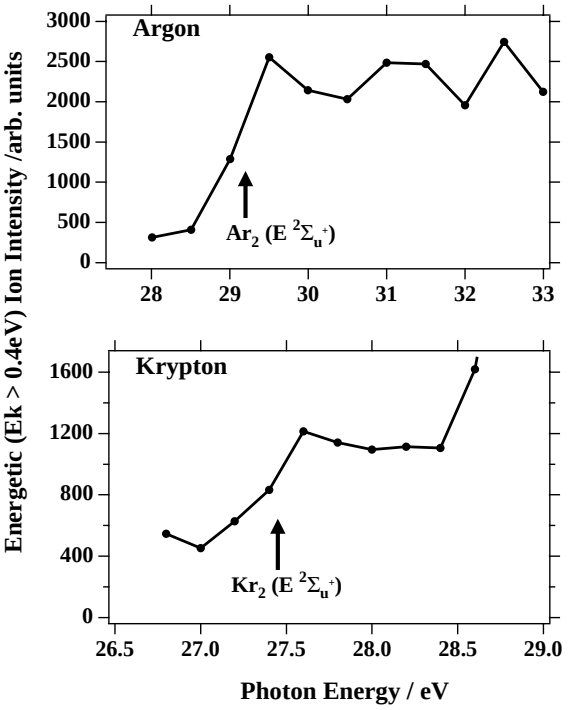


**Fig. 4.** Excitation spectra of the energetic ions (> 0.4 eV) for Ar and Kr. The position of the atomic $Rg^+(ns^{-1})$ threshold is indicated in each case.

increase in cluster size is minor; the major step seems to be already achieved in the dimer.

In Ar and Kr, similar threshold photoelectron spectra were obtained by Kamke *et al.* [20–22] who gave an extensive interpretation of the observed structure in terms of exciton formation. As our data agree very well with those presented by these authors we will not comment further on the structure present in Figure 2. We shall only point out two features of the two sets of data. First, the similarity between the threshold photoelectron spectra obtained in coincidences with dimer ions by Kamke *et al.* and the threshold photoelectron spectra of Figure 2 means that the latter effectively originate from clusters. Second, the sharp peaks attributed to the dimer in Figure 1, do not seem to be present in the data of Kamke *et al.*: this may come from the limited resolution of 80 meV used by these authors, and from their average cluster size, higher than ours, that diminishes the relative importance of this peak compared to the remainder of the spectrum. Another possibility is that the dimer peaks in Figure 1 are not coincident with the $Rg_2^+$ parent, but with a $Rg^+$ fragment, but a direct coincident measurement is clearly needed to clarify this point.

### 3.2 Measurements of the kinetic energy of the fragment ions

Typical ion kinetic energy spectra at two photon energies for each of the three rare gases are presented in Figure 3. The 0 eV thermal peak originates mainly from ionization of the isolated atoms. Figure 3 shows that energetic ions appear, in each case, for the higher of the two photon energies. A peak at $0.7 \pm 0.1$ eV is clearly resolved for Ar, but for Kr and Xe, the structure appears as a shoulder at the base of the thermal peak, located at $0.55 \pm 0.15$ eV for Kr and $0.4 \pm 0.2$ eV for Xe. These spectra were obtained under the same conditions of low stagnation pressure as in Figure 1. Increasing the stagnation pressure resulted in the appearance of signal between the 0 eV peak and the energetic one leading ultimately to a smearing out of the energetic structure. On the other hand, decreasing the stagnation pressure had the consequence of diminishing the intensity of the energetic structure relative to the 0 eV peak, without changing its overall shape. Therefore, all further measurements of ion kinetic energy were performed at the low stagnation pressure conditions of Figure 1 and the energetic component appearing in Figure 3 are interpreted as being associated with the dimer and corresponding to the kinetic energy of one rare gas atomic ion.

Figure 4 shows excitation spectra of the energetic (> 0.4 eV) ions for Kr and Ar. The low signal required that the slit widths of the monochromator be opened up to 1 mm, resulting in a photon resolution of around 0.25 eV. The threshold of the energetic ions is observed to coincide

**Table 1.** Spectroscopic values of the $E\ ^2\Sigma_u^+$ state of the $Rg_+^2$ dimer.

| Rg | Observed peak position (eV) (*this work*) | Potential well of neutral dimer $D_0$ (meV) [17] | Ionisation potential for $Rg^+(ns^{-1})$ (eV) [31] | Peak position below $Rg^+(ns^{-1})$ + Rg limit (meV) (*this work*) | Depth of $E\ ^2\Sigma_u^+$ potential well (meV) [14] |
|---|---|---|---|---|---|
| Ar | 29.197 | 9.5 | 29.240 | 52 (5) | 47 (3) |
| Kr | 27.446 | 15.7 | 27.514 | 84 (2) | 104 (22) |
| | 27.458 | | | 72 (2) | |
| Xe | 23.304 | 22.9 | 23.397 | 116 (3) | – |
| | 23.322 | | | 98 (3) | |

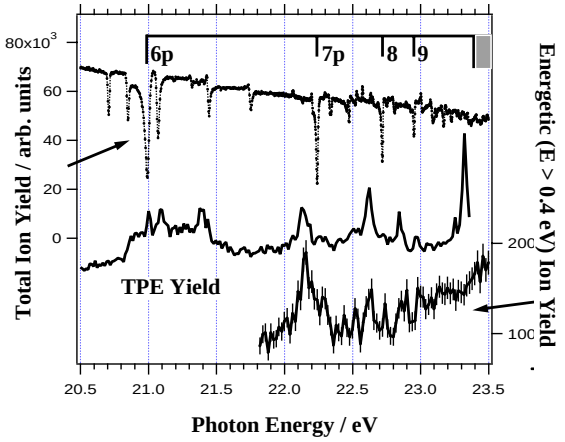


**Fig. 5.** Xenon. Bottom: excitation spectra for energetic ions ($> 0.3$ eV), with an accumulation time of 7 hours. The position of the threshold for the atomic $Xe^+(5s^{-1})$ state is indicated in the top of the figure. The upper curve gives the total ion yield, measured with a higher photon energy resolution (10 meV *versus* 60 meV) and the middle one is the low stagnation pressure, threshold electron yield of Figure 2.

with the threshold of the $E\ ^2\Sigma_u^+$ state of the dimer or with the atomic $Rg^+(ns^{-1})$ threshold which are indistinguishable at this low photon resolution. Note the non zero signal below threshold: it is attributed to the pollution by the 0 eV thermal peak and/or to the contribution of the autoionization of Rydberg states, as seen below for Xe. Better photon energy resolution could be obtained for the Xe case because of the higher efficiency of the monochromator at the lower photon energies involved. The energetic ion yields presented in Figure 5 were obtained with monochromator slit widths of 400 $\mu$m corresponding to a 60 meV photon energy resolution. Figure 5 shows that in Xe the threshold for energetic ions is below that of both the atomic $Xe^+(5s^{-1})$ state and the $E\ ^2\Sigma_u^+$ state of the dimer. This yield of energetic $Xe^+$ ions reveals structure that is attributed to the presence of resonances (see below). Also shown in Figure 5, for comparison, is the total ion yield under high resolution conditions (slits of 30 $\mu$m for a 10 meV resolution) which is essentially that of the atomic constituent in the beam. The threshold photoelectron spectrum of Figure 2 at low stagnation pressure (0.7 atm) is also shown in Figure 5.

## 4 Interpretation

### 4.1 Observation of the E $^2\Sigma_{u^+}$ state of the $Rg_2^+$ dimer

As stated in Section 3.1, we interpret the structure below the atomic line in Figure 1 as being associated with the formation at threshold of vibrational states hosted in the potential well of the weakly bound $E\ ^2\Sigma_u^+$ state of the $Rg_2^+$ dimer. Only one peak, noticeably broader than the atomic peak, is observed for Ar (Fig. 1a), whereas, for Kr and Xe, two peaks are resolved in Figures 1b and 1c, and a third one may well be present. The observed positions of these peaks are reported in Table 1. The well depth, $D_0$, of the neutral dimer ground state [17] and the ionization potential of the atomic $ns$ shell [31] are also reported in Table 1. The relative position of the observed vibrational levels with respect to the dissociation limit $Rg^+(ns^{-1})$ + Rg to which the $E\ 2\Sigma_u^+$ state is correlated can then be deduced. These values can be compared with the depth of the potential well of the $E\ ^2\Sigma_u^+$ state given by White and Grover [14]. The present results should represent a lower limit for the depths and are in qualitative agreement with those of White and Grover if the uncertainties in their method, based on an extrapolation technique, are taken into account.

### 4.2 Observation of two categories of excited states in the cluster

As mentioned in the introduction, the previous experimental and theoretical investigations had identified two different groups of excited states of the $Rg_N^+$ ionic cluster in this energy region:

1) Loosely bound states arising from the dimer $E\ ^2\Sigma_u^+$ state of Mulliken correlated to the $Rg^+(n^{-1})$ + $(N-1)$Rg limit. These states present an inner valence character and were observed in the experiments of White and Grover [14].
2) Excitonic states correlated to limits of the type: $Rg^+(np^{-1})$ + $Rg^*(ns^2\ np^5\ n'l)$ + $(N-2)$Rg. These states have a peculiar topology and Rydberg character with respect to the doubly charged $Rg_N^{++}$ cluster. They were discovered by Cachoncinlle *et al.* [16] in the $Ar_2^+$ dimer, and have been extensively studied by the group of Kamke [19–22].

The threshold photoelectron spectra of Figures 1 and 2 show that these previous observations are not incompatible: in fact, both groups of states are observed in our data, but with very different behaviours.

- In the dimer, the shallow innervalence states are "bright", that is, easily formed, whereas, on the contrary, excitonic states are "dark", and are only weakly formed in small clusters. This can be understood if we consider their main electronic configuration: the bright states correspond to a single hole configuration (hole in the $ns$ shell of one of the constituent atoms) whereas the excitonic states are described rather by a 2 hole-1 particle configuration, since at large $R$ they correspond to the excitation of one atom plus the ionization of a different atom inside the same cluster. Photoionization is known to favour, by far, one electron transitions and, consequently, creates essentially the bright valence states. Moreover, creation of an excitonic state would imply, in the above simplified description, that one atom in the cluster be ionized while a different one in the same cluster be excited, which is improbable or requires very efficient correlation mechanisms.

- As the size of the cluster increases, the excitonic states become more accessible and bright as the two electron transition process becomes more efficient. This can be explained using the simple picture wherein absorption of a photon ejects a $np$ electron from a given atom and subsequently excites another $np$ electron from a different atom inside the cluster before escaping. The probability of this secondary collision obviously increases rapidly with the size of the cluster. An equivalent explanation is with reference to correlation between electrons. The simple model above corresponds to final state correlation in this description. Electron correlation is seen to increase with the size of the cluster and is also expected to increase when going from Ar to Kr and Xe. This can explain why the exitonic states are always visible in Xe at the lowest stagnation pressure used, in spite of their dark character.

### 4.3 Predissociation of the E $^2\Sigma_u^+$ state of the $Rg_2^+$ dimer by excitonic states

In the experimental situation where the dimer signal is dominant, the observations show that the appearance of energetic ions is correlated to the creation of the $E\ ^2\Sigma_u^+$ state of the $Rg_2^+$ dimer. We propose that these energetic ions originate mainly from predissociation of the $E\ ^2\Sigma_u^+$. The measured values of the kinetic energy released in the dissociation enable us to investigate which dissociation limit is reached, and this information can be obtained from Figure 6. The relationship between the ion kinetic energy ($E_{c\ ion}$) and the dissociation limit reached, $E_{Diss\ limit}$ is given for a dimer by:

$$E_{Diss\ limit} = (\text{Binding energy of } E\ ^2\Sigma_u^+ \text{ state}) - (\text{Total kinetic energy release} = 2E_{c\ ion})$$

Thus the ion kinetic energy spectra of Figure 3 are presented in Figure 6 on a kinetic energy release (KER) scale with origin at the energy of the $v = 0$ level of the $E\ ^2\Sigma_u^+$ state where they can be compared directly to the positions of the dissociation limits into excited fragments of the type $Rg^+(np^{-1}) + Rg^*$, calculated from spectroscopic values in the literature [17,31]. Due to the possible combinations of spin-orbit components of both the neutral and the ionic fragment, many excited dissociation limits are located below the $Rg^+(ns^{-1})$ + Rg limit as can be seen. For Ar the $0.7 \pm 0.1$ eV photoion peak indicates that the $Ar^+ + Ar^*(3s^2\ 3p^5\ 4s)$ limit is efficiently populated but the low resolution does not allow either the spin-orbit status of the fragments to be determined, or the elimination of possible dissociation to the $Ar^+ + Ar^*(3s^2\ 3p^5\ 4p)$ limit that would contribute to the photoion spectrum below 0.3 eV. In contrast, in Kr, it is not the equivalent $Kr^+ + Kr^*(4s^2\ 4p^5\ 5s)$ limit that is reached, but rather more excited ones such as $Kr^+ + Kr^*(4s^2\ 4p^5\ 4d)$ or $Kr^+ + Kr^*(4s^2\ 4p^5\ 5p)$, or even $Kr^+ + Kr^*(4s^2\ 4p^5\ 6s)$. Similarly for Xe, despite the larger spin-orbit splitting, the $Xe^+ + Xe^*(5s^2\ 5p^5\ 6s)$ limit is not populated. In this case the more probable dissociation limits include $Xe^+ + Xe^*(5s^2\ 5p^5\ 5d)$ or $Xe^+ + Xe^*(5s^2\ 5p^5\ 6p)$ or $Xe^+ + Xe^*(5s^2\ 5p^5\ 7s)$. Clearly further experimental work is needed to determine precisely which limits are reached. However, within our detection efficiency, no indication of dissociation to $Rg^+(np^{-1})$ + Rg limits was found, this would have given photoion peaks near 7 eV in Ar and 6 eV in Xe. The conclusion is then that the $E\ ^2\Sigma_u^+$ state of the $Rg_2^+$ dimer is efficiently predissociated by the excitonic states, and that the precise mechanism depends on their relative positions and couplings, which change from one rare gas to another. Note that this discussion relies on our measurement of ion kinetic energies done at one photon energy (Fig. 3), just above the $E$ state threshold. Although other preliminary measurements in the threshold region showed only weak changes, more detailed investigation is clearly needed here.

The innervalence region of rare gas dimers is seen to present unique characteristics. Ionisation first creates the bright, valence $E\ ^2\Sigma_u^+$ state, corresponding to the removal of a $\sigma_u ns$ electron. Subsequently, this state is efficiently predissociated by the dark excitonic states, to which it constitutes an entrance path. This suggests that photon absorption is best described, in this case, with diabatic potential curves, but that further time evolution gives access to the adiabatic surfaces. This may explain why Cachoncinlle *et al.* [16] did not find the $E\ ^2\Sigma_u^+$ state in their adiabatic approach. An alternative reason may be that the position of the minimum of the $E\ ^2\Sigma_u^+$ state is located at internuclear distances larger than those investigated. Note also that this predissociation process implies energy transfer between the two partners in the dimer during dissociation, since the starting point is a state best described as composed of a ground state atom plus an excited ion with a hole in the $ns$ shell, and the fragmentation results in an atom in an excited state plus an ion in the electronic ground state. This interatomic coulombic mechanism can be related to the one recently predicted by Cederbaum *et al.* [32,33]: they suggest that cluster states with an innervalence electron missing can efficiently decay by a giant

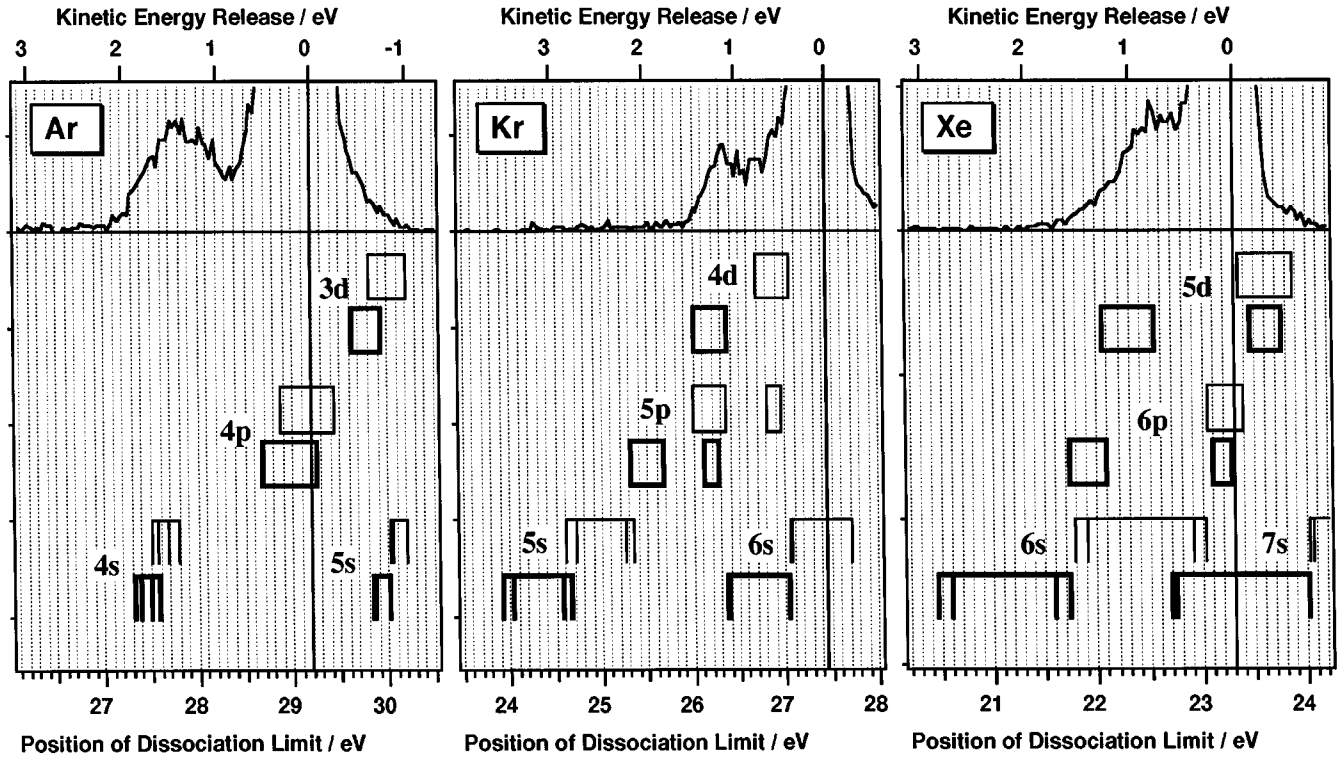


**Fig. 6.** Lower parts: position of the $Rg^+(np^{-1})$ + $Rg^*(ns^2\ np^5\ n'l)$ dissociation limits. The levels associated to $Rg^*(ns^2\ np^5\ n's)$ are represented by vertical bars; while the numerous limits corresponding to $Rg^*(ns^2\ np^5\ n'p)$ or $Rg^*(ns^2\ np^5\ n'd)$ are represented by rectangles. Thin lines correspond to limits involving a spin orbit excited ion: $Rg^+(np^{-1})\ ^2P_{1/2}$ and thick ones to a spin orbit ground state ion: $Rg^+(np^{-1})\ ^2P_{3/2}$. The upper curves are the ion kinetic energy spectra set on a Total kinetic energy release scale with origin at the $v = 0$ level of the $E\ 2\Sigma_u^+$ dimer state (dimers are assumed, see text).

intermolecular Auger decay. In our case, Auger decay is not energetically allowed, but the interatomic coulombic process we observe results, after predissociation, in the excitation of an "aborted" Auger electron, in the excited neutral fragment.

### 4.4 The $Xe_2^*$ Rydberg states converging to the E $^2\Sigma_u^+$ state of $Xe_2^+$

The total ion yield curve in Figure 5 displays almost exclusively the atomic Xe features, the most prominent being the structure corresponding to formation of the $Xe^*(5s^1\ 5p^6\ np)$ resonances. Structure related to these resonances is also present in the threshold spectrum which, as already discussed, results from processes involving the dimer. In the region above 22 eV, these resonances are mimicked in the threshold spectrum with a slight shift of about 0.1 eV towards lower energies. This immediately identifies the structure as a weakly bound resonant or Rydberg series of $Xe_2^*$, correlated to $Xe^*(5s^1\ 5p^6\ np)$ + Xe and converging to the $E\ ^2\Sigma_u^+$ state of $Xe_2^+$. The analogous $Ar_2^*$ and $Kr_2^*$ Rydberg states (correlated to $Rg^*(ns^1\ np^6\ n'p)$ + Rg) were observed previously by White and Grover [14] in the dimer ion yield. No data exists, to our knowledge, on the dimer ion yield for Xe. However, as can be clearly seen in Figure 5, these resonances are present in the energetic $Xe^+$ ion yield which has its origin in the dimer.

These observations thus indicate that the $Rg_2^*$ Rydberg states can evolve either by autoionization to the bound part of the lower "outer valence" states of $Rg_2^+$, producing the long lived $Rg_2^+$ species detected by White and Grover [14], or by autoionization to the excitonic states, in which case energetic ions can emerge, as seen here in Xe. In order to produce a threshold electron the resonant state must autoionize to a degenerate ionic state. This means that the origin of the sharp threshold electron peaks in the dimer spectrum is not due to direct formation of the excitonic states, but to an indirect process, in which the entrance step is once more a bright state, that is, a $Xe_2^*$ Rydberg state populated by a one electron $5s \rightarrow n'p$ transition.

The measured kinetic energy of the $Xe^+$ fragment ions ($0.4 \pm 0.2$ eV) is compatible with the above mechanism. But more precise measurement of the kinetic energy of these fragment ions, not possible with the present instrument, would provide interesting information on the autoionization and dissociation processes and their possible competition.

## 5 Conclusion

We observe that two classes of states dominate the inner-valence shell region of rare gas clusters: shallow valence states correlated to $Rg^+(ns^{-1}) + (N-1)Rg$ limits, and excitonic, or Rydberg states correlated to $Rg^+(np-1) + Rg^*(ns^2\ np^5\ n'l) + (N-2)Rg$. These states show very different behaviour. While valence states are readily formed in the dimer and in small clusters, excitonic states are only populated efficiently in large clusters. The small well of the $E\ ^2\Sigma_u^+$ dimer state is seen to house vibrational levels, and its depth is found to be in qualitative agreement with previous estimates.

The ion kinetic energy measurements under dimer formation conditions reveal that the appearance of energetic ions is correlated with accessibility of this $E\ ^2\Sigma_u^+$ state. It is proposed that this state is predissociated by the Rydberg states, and estimates of the ion kinetic energy suggest a different behaviour depending on the rare gas. In Ar the dissociation limit formed involves a Rydberg $Ar^*(3s^2\ 3p^5\ 4s)$ atom while, for instance, in Kr it is not the equivalent $Kr^+ + Kr^*(4s^2\ 4p^5\ 5s)$ limit but rather the $Kr^+ + Kr^*(4s^2\ 4p^5\ 4d)$ limit that is reached. This difference is ascribed to differences in the potential curves of the excited $Rg_2^+$ ion whose theoretical characteristics would be of considerable interest to know.

The authors would like to thank Y. Morioka for discussion on his preliminary investigations of this subject, as well as C. Cachoncinlle and W. Kamke for extensive discussions. R. Thissen acknowledges an EEC scholarship (Scientific Training Programme in Japan).

## References

1. P.M. Dehmer, S.T. Pratt, *Photophysics and Photochemistry in the Vacuum Ultraviolet*, edited by S.P. McGlynn *et al.*, NATO ASI Series C, Vol. 142 (Reidel, Dortrecht, 1985), p. 467.
2. P.M. Dehmer, J.L. Dehmer, J. Chem. Phys. **69**, 125 (1978).
3. T. Pradeep, B. Niu, D.A. Shirley, J. Chem. Phys. **98**, 5269 (1993).
4. Y. Morioka, H. Masuda, Y. Lu, K. Tanaka, T.Hayaishi, J. Phys. B **25**, 5343 (1992).
5. Y. Lu, Y. Morioka, T. Matsui, H. Yoshii, R.I. Hall, T. Hayaishi, K. Ito, J. Chem. Phys. **102**, 1553 (1995).
6. R.I. Hall, Y. Lu, Y. Morioka, T. Matsui, T. Tanaka, H. Yoshii, T. Hayaishi, K. Ito, J. Phys. B **28**, 2435 (1995).
7. R. Signorell, A. Wüest, F. Merkt J. Chem. Phys. **107**, 10819 (1997).
8. K. Furuya, K. Kimura, T. Hirayama, J. Chem. Phys. **97**, 1022 (1992).
9. C.A. Woodward, A.J. Stace, J. Chem. Phys. **94**, 4234 (1991); A.J. Jones, P. Jukes, A. Buxey, A.J. Stace, J. Chem. Phys. **106**, 1367 (1997) and references therein.
10. R.S. Mulliken, J. Chem. Phys. **52**, 5170 (1970).
11. H.H. Michels, R.H. Hobbs, L.A. Wright, J. Chem. Phys. **69**, 5151 (1978).
12. W.R. Wadt, J. Chem. Phys. **68**, 402 (1978).
13. F.X. Gadea, I. Paidarova, Chem. Phys. **209**, 281 (1996).
14. M.G. White, J.R. Grover, J. Chem. Phys. **79**, 4124 (1983).
15. M.C. Castex, I. Dimicoli, J. Le Calvé, F. Piuzzi, A. Tramer, *Photophysics and Photochemistry above 6 eV* (Elsevier, 1986), p. 661.
16. C. Cachoncinlle, J.M. Pouvesle, G. Durand, F. Spiegelmann, J. Chem. Phys. **96**, 6093 (1992).
17. D.E. Freeman, K. Yoshino, Y. Tanaka, J. Chem. Phys. **61**, 4880 (1974).
18. C. Cachoncinlle, J.M. Pouvesle, G. Durand, F. Spiegelmann, J. Chem. Phys. **96**, 6085 (1992).
19. H. Steger, J. de Vries, W. Kamke, I.V. Hertel, Z. Phys. D **21**, 85 (1991).
20. W. Kamke, in *Cluster Ions*, edited by C.Y. Ng, T. Baer, I. Powis (Wiley, Chichester, 1993), p. 1.
21. J. de Vries, B. Kamke, H. Steger, A. Hielscher, J. Holzapfel, U. Mische, W. Kamke, J. Chem. Phys. **101**, 9366 (1994).
22. J. de Vries, B. Kamke, H. Steger, B. Weisser, M. Honka, W. Kamke, J. Chem. Phys. **101**, 2372 (1994).
23. G. Dujardin, L. Hellner, L. Philippe, M.J. Besnard-Ramage, P. Cirkel, Phys. Rev. B **48**, 14529 (1993).
24. K. Ito, Y. Morioka, M. Ukai, N. Kouchi, Y. Hatano, T. Hayaishi, Rev. Sci. Instrum. **66**, 2119 (1995).
25. T. Tanaka, Y. Morioka, Y. Lu, T. Matsui, H. Yoshii, R.I. Hall, T. Hayaishi, J. Electron. Spectrosc. Relat. Ph. **79**, 507 (1996).
26. Y. Morioka, Y. Lu, T. Matsui, T. Tanaka, H. Yoshii, T. Hayaishi, R.I. Hall, J. Chem. Phys. **104**, 9357 (1996).
27. K. Ito, R.I. Hall, M. Ukai, J. Chem. Phys. **104**, 8449 (1996).
28. M. Ukai, M. Kitajima, S. Machida, Y. Hatano, P. Lablanquie, T. Hayaishi, K. Ito, J. Electron. Spectrosc. Relat. Ph. **79**, 471 (1996).
29. C. Moore, *Atomic energy levels*, Vol. I, II, III (US Govt. Printing Office, Washington DC, 1971).
30. J. Krauss, J. de Vries, H. Steger, E. Kaiser, B. Kamke, W. Kamke, Z. Phys. D **20**, 29 (1991).
31. O.F. Hagena, Z. Phys. D **4**, 291 (1987).
32. L.S. Cederbaum, J. Zobeley, F. Tarantelli, Phys. Rev. Lett. **79**, 4778 (1997).
33. J. Zobeley, L.S. Cederbaum, F. Tarantelli, J. Chem. Phys. **108**, 9737 (1998).